Check for updates

Geophysical Research Letters

RESEARCH LETTER
10.1029/2025GL119526

Mesoscale Eddy Currents Reshape the Spatial Distribution of Wave Height in the Southern Ocean

Tianyi Cheng[1,2], Zhaohui Chen[1], Jingkai Li[1], and Alexander V. Babanin[2]

[1]Frontier Science Center for Deep Ocean Multispheres and Earth System (FDOMES) and Physical Oceanography Laboratory, Ocean University of China, Qingdao, China, [2]Department of Infrastructure Engineering, University of Melbourne, Parkville, VIC, Australia

Key Points:

- Wave height increases (decreases) on the side where waves propagate against (with) eddy currents, forming a dipole pattern
- Typical eddy currents of 0.15 m s^{-1} with a radius of 45 km cause wave height changes of about 5 cm
- Numerical simulations show that refraction is the dominant mechanism by which mesoscale eddy currents redistribute wave energy

Supporting Information:

Supporting Information may be found in the online version of this article.

Correspondence to:

Z. Chen,
chenzhaohui@ouc.edu.cn

Citation:

Cheng, T., Chen, Z., Li, J., & Babanin, A. V. (2026). Mesoscale eddy currents reshape the spatial distribution of wave height in the Southern Ocean. *Geophysical Research Letters*, *53*, e2025GL119526. https://doi.org/10.1029/2025GL119526

Received 18 SEP 2025
Accepted 31 MAR 2026

Author Contributions:

Conceptualization: Zhaohui Chen
Data curation: Tianyi Cheng
Formal analysis: Tianyi Cheng
Funding acquisition: Zhaohui Chen
Investigation: Tianyi Cheng
Methodology: Tianyi Cheng, Zhaohui Chen, Jingkai Li
Supervision: Zhaohui Chen, Jingkai Li, Alexander V. Babanin
Visualization: Tianyi Cheng
Writing – original draft: Tianyi Cheng, Zhaohui Chen, Jingkai Li
Writing – review & editing: Tianyi Cheng, Zhaohui Chen, Jingkai Li, Alexander V. Babanin

© 2026 The Author(s).
This is an open access article under the terms of the Creative Commons Attribution-NonCommercial License, which permits use, distribution and reproduction in any medium, provided the original work is properly cited and is not used for commercial purposes.

Abstract Mesoscale eddy currents influence ocean surface waves, but their imprints on wave height remain poorly described by observations. Here, we examine significant wave height (SWH) variations associated with more than 42,000 mesoscale eddies in the Southern Ocean using along-track Jason-3 altimeter measurements. Altimeter composites reveal a pronounced meridional dipole, with reduced SWH where wave propagation aligns with eddy currents and enhanced SWH on the opposing side. Typical eddies (radius ~45 km, geostrophic velocity anomalies ~0.15 m s^{-1}) are associated with SWH anomalies of ~5 cm. Reanalysis data and idealized simulations further suggest that eddy-related wind anomalies, the relative wind effect and direct current effects all contribute to the observed SWH patterns, with refraction playing a key role. These results highlight the role of mesoscale currents in redistributing wave energy and shaping the spatial distribution of wave height.

Plain Language Summary Ocean waves travel across the sea surface and are influenced by both winds and ocean currents. One type of current, called a mesoscale eddy, is a large rotating feature that typically spans tens to hundreds of kilometers. In this study, we analyzed satellite observations from more than 42,000 cases in which waves passed through such eddies in the Southern Ocean. We found that eddies are associated with changes in wave height: waves tend to be lower where they propagate with the current and higher where they propagate against it. For typical eddies about 45 km in radius with current speeds of around 0.15 m s^{-1}, these changes are about 5 cm. We further use wave reanalysis data and idealized simulations to help explain the observed patterns. Together, they show that mesoscale eddies affect wind waves and swell in different ways, and that eddy currents can directly change wave height, with wave refraction playing an especially important role.

1. Introduction

Mesoscale eddies are ubiquitous in the global ocean, and their characteristics and impacts on oceanic and atmospheric processes have been extensively investigated using satellite observations (Chelton et al., 2011; Chen et al., 2019; Frenger et al., 2013; He et al., 2016; Wang et al., 2023). However, their effects on wave height remain insufficiently quantified, largely due to limited in situ wave observations in open oceans and the asynchronous spatial coverage of satellite altimeter data, both of which hinder the detection of eddy-induced wave variability. Mesoscale eddies may influence wave height through multiple pathways. Eddy-associated geostrophic velocity anomaly (GVA) can modify wave frequency and propagation direction (Ardhuin et al., 2017), while eddy-induced sea surface temperature (SST) anomalies can modulate surface winds (Frenger et al., 2013), a primary driver of wave generation (Janssen, 1991). Together, anomalies in surface winds and geostrophic currents may affect wave height throughout wave evolution, with potential impacts on extreme sea states (Echevarria et al., 2021).

Most existing studies of eddy effects on wave height rely on numerical models. Simulations suggest that ocean currents at scales of 10–100 km can contribute to significant wave height (SWH) variability in the open ocean (Ardhuin et al., 2017). In particular, wave refraction over mesoscale eddies can cause convergence and divergence of wave energy, resulting in corresponding changes in SWH (Marechal & de Marez, 2022). Observational evidence remains limited. Satellite altimeter analyses have revealed mesoscale spatial patterns in SWH (Quilfen & Chapron, 2019), and measurements from the Surface Wave Investigation and Monitoring (SWIM) antenna onboard the Chinese-French Oceanography Satellite (CFOSAT) indicate that eddy-induced surface wind anomalies may modulate wave height (Hauser et al., 2017; Tan et al., 2023). Nevertheless, large-sample observational characterizations of eddy-related SWH variability are still lacking.

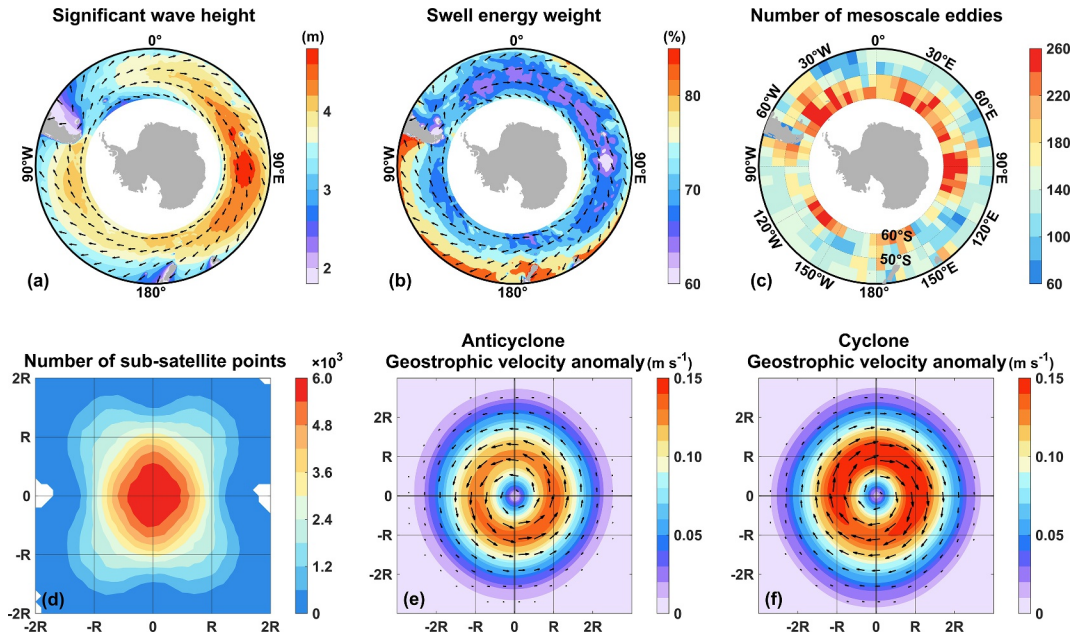

Figure 1. (a, b) Multi-year mean wave fields in the Southern Ocean (60°S–40°S) during 2016–2019: (a) significant wave height with overlaid peak wave direction; (b) ratio of swell energy to total wave energy with overlaid primary swell direction. (c, d) Spatial distributions of mesoscale eddy occurrences and satellite sampling during 2016–2019: (c) number of mesoscale eddies observed by Jason-3, binned onto 5° × 5° grids; (d) number of satellite sampling points in a normalized eddy-centered coordinate system scaled by the eddy radius (R), aggregated within 0.1R × 0.1R bins. Composite surface geostrophic velocity anomalies associated with the above detected (e) anticyclonic and (f) cyclonic eddies.

The Southern Ocean features a circumpolar circulation linking the major ocean basins and, together with strong and persistent westerly winds, supports the generation of highly energetic wave fields (Hanley et al., 2010). South of 40°S, the prevailing wave direction is generally from the west, gradually turning more northward at lower latitudes as Southern Ocean swells propagate into the Indian, Pacific, and South Atlantic Oceans (Figures 1a and 1b; Casas-Prat et al., 2024; Young et al., 2020). Meanwhile, the Antarctic Circumpolar Current dominates the regional circulation, making the Southern Ocean one of the most eddy-rich regions in the global ocean (Patara et al., 2016). Therefore, the concurrence of energetic waves and abundant mesoscale eddies makes the Southern Ocean particularly well suited for investigating how eddy currents redistribute wave energy.

Here, we analyze more than 42,000 mesoscale eddies in the Southern Ocean (60°S–40°S) from 2016 to 2019 (Figures 1c–1f), using 1-Hz along-track wind speed and SWH measurements from the Jason-3 altimeter, with a nominal sampling interval of ∼6 km. Our primary aim is to characterize and quantify the spatial patterns of eddy-related wave height variability based on altimeter observations. To further examine the contributions of different wave components, wave reanalysis data are employed to separate wind wave and swell responses. Idealized numerical simulations are used to diagnose the direct effects of currents on wave height through wave-current interaction mechanisms.

2. Data and Method

2.1. Data Collection

We used Level 2 Geophysical Data Records from the Jason-3 altimeter, providing SWH and 10-m wind speed at 1 Hz, corresponding to an along-track sampling interval of approximately 6 km. Altimeter-derived SWH corresponds to four times the standard deviation of sea surface elevation (Fedor & Brown, 1982). Jason-3 wind speed is retrieved from Ku-band backscatter using a geophysical model function based on the approach of Gourrion et al. (2002). Data quality was ensured through standard mission quality flags and the additional criteria of Zieger et al. (2009) to remove low-quality measurements and outliers.

19448007, 2026, 8, Downloaded from https://agupubs.onlinelibrary.wiley.com/doi/10.1029/2025GL119526 by Zhaohui Chen - Ocean University Of China , Wiley Online Library on [11/04/2026]. See the Terms and Conditions (https://onlinelibrary.wiley.com/terms-and-conditions) on Wiley Online Library for rules of use; OA articles are governed by the applicable Creative Commons License

19448007, 2026, 8, Downloaded from https://agupubs.onlinelibrary.wiley.com/doi/10.1029/2025GL119526 by Zhaohui Chen - Ocean University Of China , Wiley Online Library on [11/04/2026]. See the Terms and Conditions (https://onlinelibrary.wiley.com/terms-and-conditions) on Wiley Online Library for rules of use; OA articles are governed by the applicable Creative Commons License

To isolate mesoscale eddy-induced SWH variability, we removed the large-scale background field represented by the AVISO 1° × 1° Gridded Wind/Wave Product, which captures variability at spatial scales of order 100 km and larger. The gridded wind speed and SWH were interpolated in space and time to the Jason-3 sub-satellite locations and subtracted from the along-track measurements. This gridded product merges wave observations from Envisat, Jason-1/2/3, AltiKa, and Sentinel-3A, and wind observations from Envisat, Jason-1/2/3, and Sentinel-3A. Our analysis focuses on the period from February 2016 to December 2019, covering the time during which the along-track and gridded satellite data overlap.

Mesoscale eddies were identified from the Mesoscale Eddy Trajectory Atlas (META3.2 DT), which detects eddies based on closed contours of absolute dynamic topography (Pegliasco et al., 2022). The eddy center and radius (R) were determined from the best-fit circle to the contour of maximum circum-average geostrophic speed. Between February 2016 and December 2019, ∼68,000 individual eddies were passed over by the Jason-3 altimeter between 60°S and 40°S. To ensure reliable eddy sampling, we selected satellite tracks passing within 40 km of the eddy center and excluded regions influenced by multiple overlapping eddies. To minimize wind field heterogeneity, only cases with wind speed and direction differences $\leq$5 m s^{-1} and $\leq$120°, respectively, between eddy interior and exterior were retained (see Figure S1 in Supporting Information S1 for the definition of eddy interior and exterior regions). As mesoscale eddies typically induce wind speed anomalies on the order of decimeters per second (Frenger et al., 2013; Ma et al., 2015), larger differences beyond these thresholds are more likely attributable to synoptic-scale atmospheric variability than to eddy effects (Lin et al., 2018; Pérez-Santos et al., 2019). After applying these filters, ∼42,000 individual eddies were used for further analysis (Figure 1c).

Two Level-4 (L4) data sets from the Copernicus Marine Service (CMEMS) are used in this study. Mesoscale eddies were characterized using 1/8° daily geostrophic velocity anomalies (GVAs) from the Global Ocean Gridded L4 Sea Surface Heights and Derived Variables Reprocessed 1993 Ongoing data set (Pujol et al., 2016), with anomalies referenced to a 20-year mean (1993–2012). To characterize the spatial distribution of waves in the Southern Ocean, significant wave height, peak wave period and peak wave direction were obtained from the Global Ocean Waves Reanalysis (WAVERYS). WAVERYS provides wave data at 1/5° resolution and 3-hourly intervals. It assimilates satellite altimeter observations together with directional wave spectra derived from Sentinel-1 synthetic aperture radar, and accounts for wave-current interactions (Law-Chune et al., 2021).

2.2. Composite Analysis

Composite analysis was applied to quantify the responses of SWH and wind speed to mesoscale eddies. Because the incoming wave direction varies among eddies and is not always zonal (270° or 90° in nautical convention; Figure S2 in Supporting Information S1), a rotated, wave-following coordinate system was adopted. For each eddy, the eddy center was defined as the origin. For Jason-3 along-track data, distances between the sub-satellite points and the eddy center were normalized by the eddy radius R. The northern (positive) and southern (negative) sides were defined relative to the wave propagation direction, yielding normalized SWH distributions (Figures S3a–S3c in Supporting Information S1). SWH at the center was obtained by linear interpolation between the two sub-satellite points closest to the eddy center, and SWH anomalies were derived by subtracting the eddy-center value (Figure S3d in Supporting Information S1). All 42,000 eddy cases were then composited to obtain the mean SWH anomalies. The same procedure was applied to along-track wind speed. The 95% confidence intervals were estimated assuming independent sampling as Mean $\pm$ 1.96 $\times \frac{\mathrm{STD}}{\sqrt{n}}$, where STD is the standard deviation and n is the sample size.

For the gridded two-dimensional data, spatial coordinates were normalized by the eddy radius and centered on the eddy center. All eddy cases were composited to obtain mean spatial fields. This procedure was applied to derive the structures of eddy GVAs and the spatial distributions of total, wind wave, and swell SWHs under eddy influence. Before compositing the wave fields, all maps were rotated to align the eastward wave propagation direction.

2.3. Effects of Currents on Waves in the SWAN Model

The third-generation wave model SWAN (version 41.51) is employed to investigate how eddy currents modulate wave height (Booij et al., 1996). The wave field is represented by the two-dimensional wave action spectrum

19448007, 2026, 8, Downloaded from https://agupubs.onlinelibrary.wiley.com/doi/10.1029/2025GL119526 by Zhaohui Chen - Ocean University Of China , Wiley Online Library on [11/04/2026]. See the Terms and Conditions (https://onlinelibrary.wiley.com/terms-and-conditions) on Wiley Online Library for rules of use; OA articles are governed by the applicable Creative Commons License

$N(\vec{x}, t; \sigma, \theta)$, distributed over intrinsic frequencies σ and propagation directions θ, and evolving in space $\vec{x}$ and time t according to (Komen et al., 1994)

$$\frac{\partial N}{\partial t} + \nabla_{\vec{x}} \cdot [(\vec{c}_g + \vec{u}) N] + \frac{\partial c_\sigma N}{\partial \sigma} + \frac{\partial c_\theta N}{\partial \theta} = \frac{S_{\text{tot}}}{\sigma} \quad (1)$$

The second term describes the advection of wave action by the group velocity $\vec{c}_g = \partial\sigma/\partial\vec{k}$ and the ambient current $\vec{u}$, where $\vec{k}$ is the wave number vector. The third and fourth terms represent frequency shifting and refraction induced by currents and depth variations (Tolman, 1990). S_{tot} is the sum of the energy source and sink terms that represent the interactions with winds, bottom, wave-wave interactions, and dissipation.

From Equation 1, the effects of currents on waves can be summarized as:

1. Advection of wave action at the velocity $\vec{c}_g + \vec{u}$.
2. Frequency shifting, accompanied by wave stretching or compression.
3. Refraction, associated with changes in wave propagation direction.
4. Modification of wind input S_{in} (relative wind effect), since S_{in} is a function of the wind speed relative to the current speed. Here $\vec{U}_{10}$ denotes the 10-m wind velocity vector. Typically, $\vec{U}_{10} - a\vec{u}$ with $a = 0$ when neglecting the current, and $a = 1$ for a full effect of the current, which neglects the adjustment of the atmosphere to the surface current velocity (Ardhuin et al., 2017; Hersbach & Bidlot, 2008).

In this study, mesoscale eddy effects on wave heights are decomposed into current-related and wind-related processes. The idealized numerical experiments focus on the current-related mechanisms, and sensitivity experiments were conducted by selectively deactivating advection, frequency shifting, and refraction to quantify their respective contributions.

All simulations were performed in nonstationary mode on a Cartesian grid of 480 km × 480 km with a spatial resolution of 4 km × 4 km and a uniform water depth of 4,000 m. The model was integrated for 2 days with a time step of 2 min. The directional wave spectrum was discretized into 48 directions and 32 frequencies spanning 0.0418–1.0 Hz. Simulations were conducted without wind forcing using the same uniform incident swell field (SWH = 3.2 m, peak period = 11.5 s, peak direction = 270° in nautical convention) propagating through eddy currents shown in Figure S4 of Supporting Information S1. The initial directional wave spectrum was defined using a JONSWAP spectrum ($\gamma = 3.3$).

3. Results

3.1. Statistical Characteristics of Wind Speed and SWH Influenced by Mesoscale Eddies

Derived from the composite of more than 42,000 mesoscale eddies in the Southern Ocean, the representative eddies reach a maximum GVA of approximately 0.15 m s^{-1} (Figures 1e and 1f). These magnitudes are comparable to those reported in other regions of vigorous eddy activity, including the North Atlantic subtropical gyre (Amores et al., 2017) and the Kuroshio Extension (Sun et al., 2017). The mean radii of anticyclonic and cyclonic eddies are 47.8 km and 45.0 km, respectively. Using Jason-3 along-track measurements, we quantified eddy-induced anomalies in wind speed and SWH after subtracting the background fields. Eddy realizations were further stratified by background wind speed and maximum GVA, each classified into above-mean and below-mean categories (Figure 2).

Statistically, anticyclonic (cyclonic) mesoscale eddies are associated with accelerated (decelerated) sea surface wind speeds near their centers. Under conditions of strong background winds (wind speed >10 m s^{-1}) and intense eddy currents (maximum GVA >0.15 m s^{-1}), the wind speed anomalies become most pronounced, with wind speeds at the eddy center differing from those at its outer edge by about 0.3 m s^{-1} (Figures 2c and 2g). Similar wind anomalies over mesoscale eddies have been reported previously (Frenger et al., 2013; Ma et al., 2015) and have been interpreted as reflecting SST-driven atmospheric adjustment processes, including downward momentum transport and pressure adjustment (Lindzen & Nigam, 1987; Wallace et al., 1989).

Notably, the wind speed extremum is displaced north of the eddy center, with cyclonic eddies exhibiting a particularly clear northward shift of about 0.5R (Figures 2g and 2h). Although this feature was also noted by Frenger et al. (2013), it has received little detailed discussion. Here, we interpret this displacement as likely

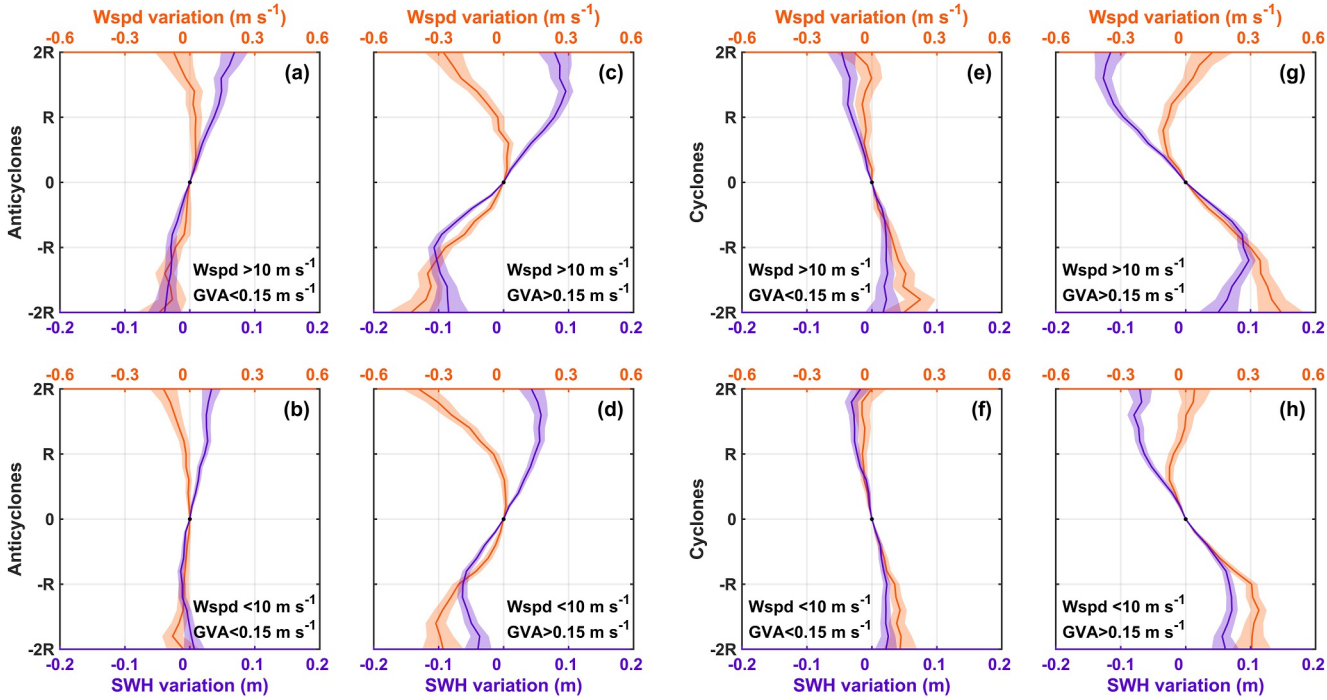

Figure 2. Variations of significant wave height (SWH) and wind speed (Wspd) from Jason-3 along-track measurements relative to the eddy center. Panels (a–d) and (e–h) show anticyclonic and cyclonic eddies, respectively, between 60°S and 40°S. Northern (+R) and southern (−R) sides, defined relative to the wave propagation direction, are shown separately in each panel. Large-scale background SWH and wind speed derived from the 1° × 1° AVISO gridded product have been removed. The composites are stratified by background wind speed and maximum geostrophic velocity anomaly (GVA), each divided into two categories relative to their respective mean values. Purple and orange denote SWH and wind speed, respectively. Solid lines indicate the composite mean, and shaded areas show the 95% confidence intervals.

arising from the combined influence of (a) absolute atmospheric adjustment to eddy-induced SST anomalies, which would in principle be centered on the eddy core, and (b) biases in satellite wind retrievals associated with eddy surface currents, as previously recognized by scatterometer-based studies (Souza et al., 2014).

Satellite microwave sensors measure winds relative to the moving ocean surface, rather than the absolute atmospheric wind. Consequently, wind speeds are underestimated when the surface wind is aligned with the ocean current, and overestimated when they oppose each other (Cheng et al., 2023; Dickinson et al., 2001; Kelly et al., 2001). In the Southern Ocean, prevailing westerlies interact asymmetrically with eddy currents: north of a cyclonic (anticyclonic) eddy, the eddy current is aligned with (opposed to) the westerlies, producing a negative (positive) bias in satellite-derived wind speeds. Together with absolute atmospheric adjustment due to eddy-induced SST anomalies, this explains the northward displacement of wind-speed extrema relative to the eddy center. This interpretation is supported by the stronger GVAs on the northern side of cyclonic eddies (Figure 1f), which enhance the relative-wind effect and amplify the displacement.

SWH variations around eddies exhibit a clear dipole pattern: SWH increases on the northern side and decreases on the southern side of anticyclonic eddies, with the opposite pattern for cyclonic eddies. The SWH response intensifies with increasing background wind speed and eddy current strength (Figure 2). Wave height changes are most pronounced near the maximum zonal GVA, with the north-south difference reaching ∼20 cm (Figures 2c and 2g). For all ∼42,000 eddies, the mean composite shows that mesoscale eddies with GVAs of ∼0.15 m s^{-1} and a mean radius of ∼45 km induce SWH anomalies of about 5 cm (Figures 3a and 3b).

Because mesoscale eddies may influence wind waves and swell through different physical mechanisms, it is important to examine their responses separately. However, Jason-3 altimetry provides along-track observations, limiting the construction of spatially continuous two-dimensional composites. In addition, the altimeter-derived SWH represents total wave height and does not robustly separate wind wave and swell components. We therefore complement the altimeter analysis with WAVERYS reanalysis, which provides spatially continuous wave fields suitable for two-dimensional compositing and wave partitioning. WAVERYS assimilates multiple satellite

19448007, 2026, 8, Downloaded from https://agupubs.onlinelibrary.wiley.com/doi/10.1029/2025GL119526 by Zhaohui Chen - Ocean University Of China , Wiley Online Library on [11/04/2026]. See the Terms and Conditions (https://onlinelibrary.wiley.com/terms-and-conditions) on Wiley Online Library for rules of use; OA articles are governed by the applicable Creative Commons License

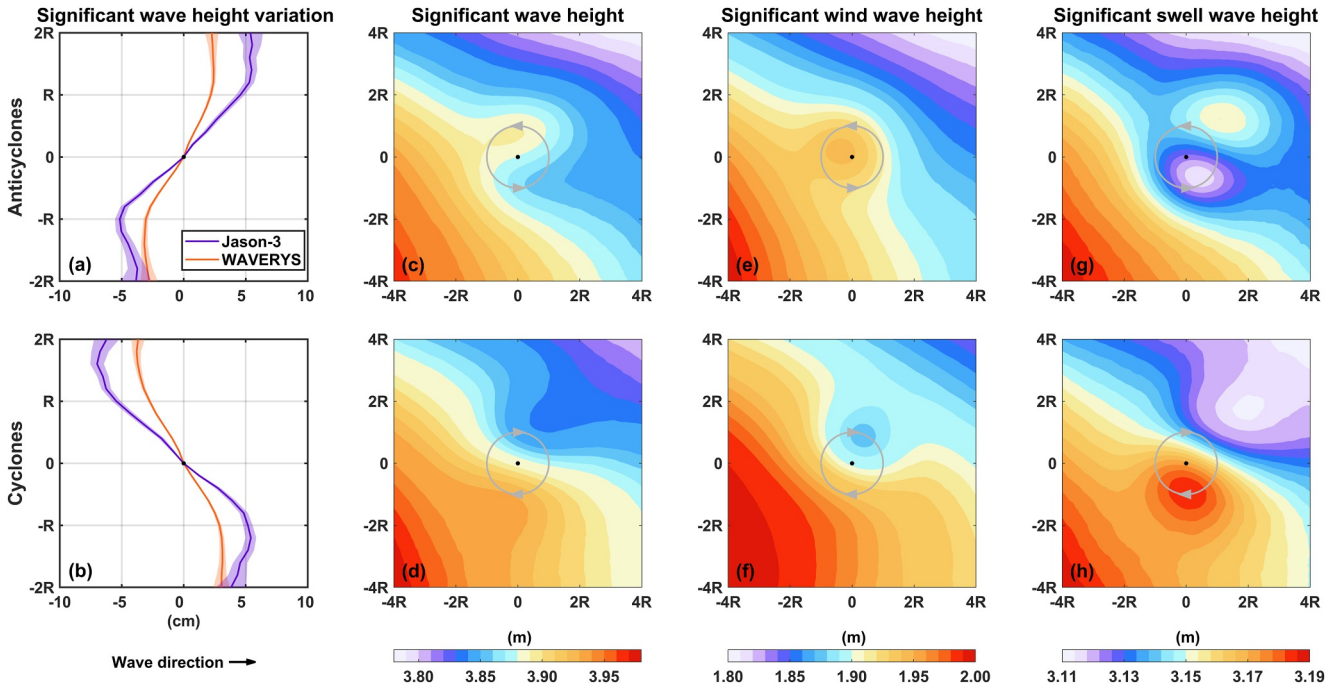

Figure 3. Mesoscale eddy imprints on significant wave height (SWH) based on ~42,000 individual eddies in the Southern Ocean (60°S–40°S), separated into (a, c, e, g) anticyclones and (b, d, f, h) cyclones. (a, b) SWH variations relative to the eddy center for the northern (+R) and southern (−R) sides, defined relative to the wave propagation direction. Purple and orange lines denote SWH from Jason-3 observations and WAVERYS reanalysis, respectively. Large-scale background SWH derived from the 1° × 1° AVISO gridded product have been removed. Solid lines indicate the mean over all eddy cases, and shaded areas represent the 95% confidence intervals. (c, d) Total SWH, (e, f) wind wave SWH, and (g, h) swell SWH from the WAVERYS reanalysis. Black dots mark the eddy centers, and gray circles denote the eddy boundaries defined by the maximum geostrophic velocity anomalies, with arrows indicating their rotation directions. Prior to compositing, wave fields were mapped onto an eddy-centered coordinate system, scaled by the eddy radius (R), interpolated onto a common grid, and rotated so that the incoming waves propagate from west to east.

observations and accounts for wave-current interactions, and its SWH agrees well with Jason-3 in the Southern Ocean (60°S–40°S), with a mean bias of 3 cm and a correlation coefficient of 0.99. Interpolating WAVERYS SWH onto the Jason-3 sub-satellite points and applying the same composite analysis reveals that WAVERYS captures the dipole-like eddy imprint, although the amplitude is smoother (2–3 cm) than that observed by Jason-3 (Figures 3a and 3b).

We further performed two-dimensional spatial composite analyses of total, wind wave, and swell SWH from WAVERYS. The background wave field consists of ~2 m wind wave SWH and ~3.2 m swell SWH and exhibits a southwest-to-northeast decreasing gradient (Figures 3c–3h). Wind wave SWH anomalies display a meridional structure closely matching the wind speed anomalies shown in Figures 2c and 2g, suggesting a combined influence of eddy-induced absolute wind anomalies and the relative wind effect, as discussed in previous studies (Echevarria et al., 2021; Tan et al., 2023). This combined influence may help explain the enhanced (reduced) wave heights within anticyclonic (cyclonic) eddies and the northward shift of the strongest SWH anomaly (Figures 3e and 3f). For swell, eddy currents generate a dipolar SWH pattern, but the amplitude is not symmetric with respect to the wave-propagation direction. Instead, it aligns with the background swell SWH gradient (Figures 3g and 3h). Overall, the total SWH exhibits an out-of-phase spatial pattern (Figures 3c and 3d), emerging from the distinct responses of wind waves and swell to eddy-related wind and current anomalies.

3.2. Numerical Diagnosis of Mechanisms Behind Eddy Current Effects on SWH

Ocean currents modify waves through advection, frequency shifting, and refraction. Among these processes, refraction has been suggested to play a leading role in shaping wave height variability from meso- to submesoscales. At the mesoscales, Marechal and de Marez (2022) reported downstream wave ray focusing and enhanced wave heights associated with refraction. Here downstream (upstream) refers to the region encountered by the swell after (before) crossing a transect through the eddy center that is perpendicular to the wave

19448007, 2026, 8, Downloaded from https://agupubs.onlinelibrary.wiley.com/doi/10.1029/2025GL119526 by Zhaohui Chen - Ocean University Of China , Wiley Online Library on [11/04/2026]. See the Terms and Conditions (https://onlinelibrary.wiley.com/terms-and-conditions) on Wiley Online Library for rules of use; OA articles are governed by the applicable Creative Commons License

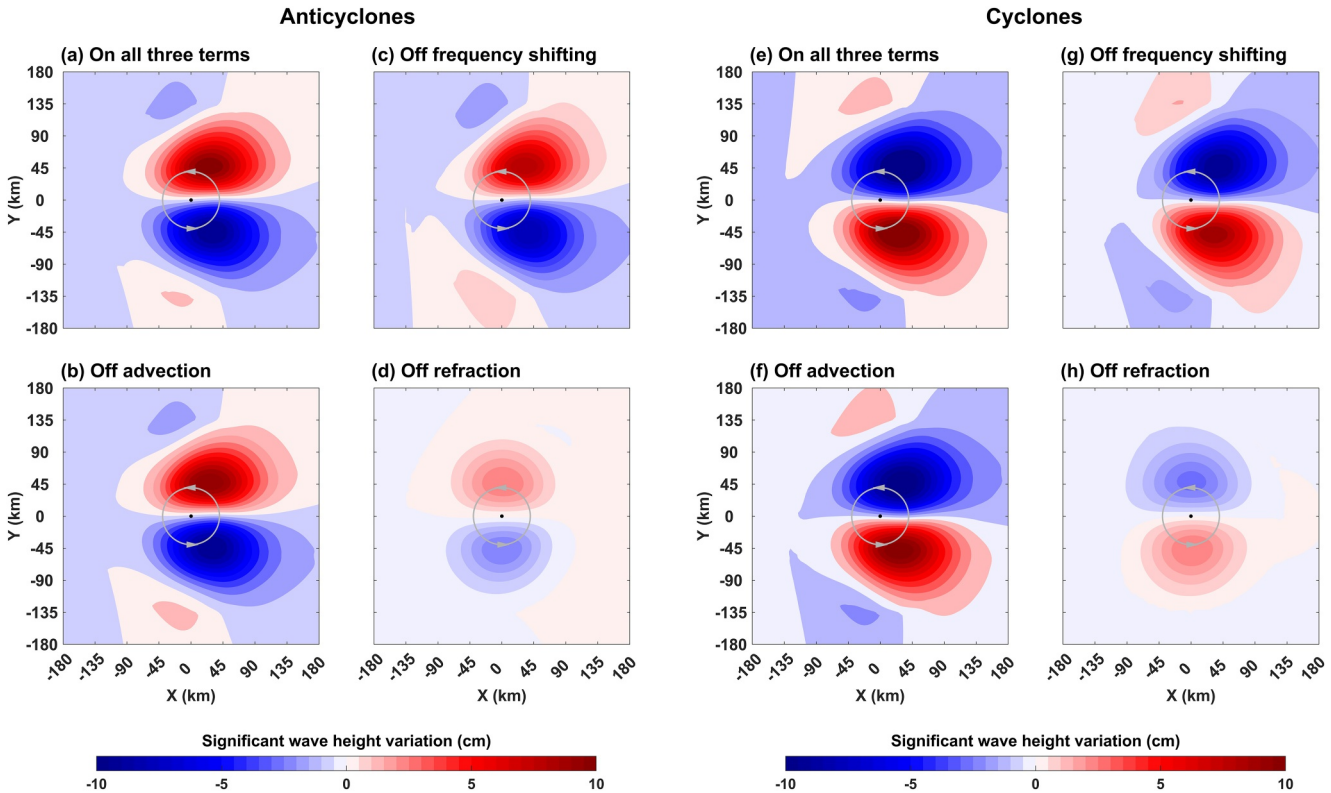

Figure 4. Variations in significant swell wave height (SWH) induced by (a–d) anticyclonic and (e–h) cyclonic eddy currents. (a, e) All current-related processes included (advection, frequency shifting, and refraction). Results from sensitivity experiments with (b, f) advection, (c, g) frequency shifting, and (d, h) refraction individually deactivated. The prescribed swell (SWH = 3.2 m, peak period = 11.5 s, peak direction = 270° in nautical convention) propagates eastward through mesoscale eddies with a 45 km radius and maximum geostrophic velocity anomaly of ∼0.15 m s^{-1}. Black dots mark the eddy centers, and gray circles denote the eddy boundaries defined by the maximum GVAs, with arrows indicating their rotation directions.

propagation direction. Consistent with this interpretation, the WAVERYS reanalysis shows that the strongest SWH anomalies occur downstream of the maximum GVA (Figures 3g and 3h). At submesoscales, Villas Bôas et al. (2020) similarly found that vorticity-induced refraction plays a major role in generating SWH gradients.

While wave reanalysis represents the spatial structure of eddy-related wave height variability under realistic atmospheric forcing, it does not permit isolation of individual wave-current interaction mechanisms. We therefore use idealized SWAN simulations, without local wind forcing, to explicitly disentangle the roles of advection, frequency shifting and refraction in eddy-induced wave height variability. We impose an incoming prescribed swell and eddy current fields derived from the composite of ∼42,000 Southern Ocean eddies. The swell (SWH = 3.2 m, peak period = 11.5 s) propagates eastward through an anticyclonic or cyclonic eddy with a radius of 45 km and a maximum GVA of ∼0.15 m s^{-1} (Figure S4 in Supporting Information S1). The simulations reproduce the strongest SWH anomalies downstream of the maximum GVA (Figures 4a and 4e). When refraction is deactivated, these anomalies are substantially reduced (Figures 4d and 4h), supporting the interpretation that wave refraction plays a primary role in the simulated SWH response.

The idealized SWAN experiments impose a single-direction, narrow-band swell propagating through a steady eddy to isolate the dominant physical mechanisms by which mesoscale eddies redistribute wave energy. Under these controlled conditions, refraction-induced focusing is more pronounced than in the WAVERYS-based composite analysis (Figures 3g and 3h), leading to SWH anomalies of up to 10 cm (Figures 4a and 4e). In contrast, the composite analysis averages a multi-directional, broadband wave field and involves spatial interpolation in the eddy-centered reference frame, which smooths small-scale variability. Despite reduced amplitudes, the dipole swell SWH pattern persists across both eddy polarities in the WAVERYS composite, indicating a generic role of mesoscale eddy-induced wave refraction.

19448007, 2026, 8, Downloaded from https://agupubs.onlinelibrary.wiley.com/doi/10.1029/2025GL119526 by Zhaohui Chen - Ocean University Of China , Wiley Online Library on [11/04/2026]. See the Terms and Conditions (https://onlinelibrary.wiley.com/terms-and-conditions) on Wiley Online Library for rules of use; OA articles are governed by the applicable Creative Commons License

19448007, 2026, 8, Downloaded from https://agupubs.onlinelibrary.wiley.com/doi/10.1029/2025GL119526 by Zhaohui Chen - Ocean University Of China , Wiley Online Library on [11/04/2026]. See the Terms and Conditions (https://onlinelibrary.wiley.com/terms-and-conditions) on Wiley Online Library for rules of use; OA articles are governed by the applicable Creative Commons License

4. Conclusion and Discussion

Our analysis of more than 42,000 mesoscale eddies in the Southern Ocean shows that eddy currents are associated with systematic changes in the spatial distribution of SWH. Composite results reveal a robust dipole pattern, with reduced SWH where wave propagation aligns with eddy currents and enhanced SWH on the opposing side. A typical Southern Ocean eddy, characterized by currents of ∼0.15 m s^{-1} and a radius of ∼45 km, induces SWH anomalies of ∼5 cm.

The wind wave SWH anomalies exhibit patterns that are consistent with the wind speed anomalies, suggesting a combined influence of eddy-induced absolute wind anomalies and the relative wind effect. In contrast, the swell SWH anomalies are primarily associated with current-induced modulation, producing out-of-phase SWH variations perpendicular to the wave propagation direction. Idealized numerical experiments further show that, among the direct effects of currents on waves, wave refraction induced by mesoscale vorticity is the dominant mechanism modulating swell wave height.

These results extend previous knowledge by providing large-sample observational evidence of mesoscale eddy imprints on waves in the Southern Ocean, complemented by reanalysis data and idealized modeling to isolate the underlying physical processes. Nevertheless, several limitations should be acknowledged. Although individual altimeter measurements contain non-negligible uncertainties (∼0.12 m for SWH and ∼0.9 m s^{-1} for wind speed) (Bignalet-Cazalet et al., 2021), these errors are largely random and are substantially reduced through compositing a large number of eddies. Consequently, the dipole-shaped SWH anomaly consistently emerges across different background wind and eddy current regimes as a coherent and statistically robust mesoscale signal, rather than an artifact of measurement noise (Figure 2). Although Jason-3 provides relatively fine along-track sampling interval (∼6 km), its wide cross-track spacing and 10-day repeat cycle limit two-dimensional coverage and may miss short-lived SWH anomalies. Nevertheless, cross-validation with reanalysis data indicates that these limitations do not alter the spatial structure or sign of the eddy-induced SWH anomalies.

Finally, our findings reflect the dynamical regime of the open Southern Ocean; in coastal or semi-enclosed basins with different bathymetry and wave spectra, the dominant mechanisms may differ. Extending this framework to other regions will enable systematic inter-basin comparisons and a broader perspective on global eddy-wave interactions.

Conflict of Interest

The authors declare no conflicts of interest relevant to this study.

Availability Statement

This study relies solely on publicly available data sets. The along-track Jason-3 Geophysical Data Records (GDRs) are obtained from AVISO (2021). Gridded wind and wave products are obtained from AVISO (2020). Mesoscale eddies are identified using the Mesoscale Eddy Trajectory Atlas Product (META3.2 DT; AVISO, 2022). Additional data sets are obtained from CMEMS, including the Global Ocean Gridded L4 Sea Surface Heights and Derived Variables data set (CMEMS, 2025a) and the Global Ocean Waves Reanalysis product (CMEMS, 2025b). Analysis codes are publicly available via figshare (Cheng et al., 2025).

Acknowledgments
Z. C. was supported by the National Natural Science Foundation of China (42225601) and Supporting Funds for Leading Talents (2022GJJLJRC02-014). T. C. was supported by Fundamental Research Funds for the Central Universities (202261001). J. L. was supported by Fundamental Research Funds for the Central Universities (202262005).

References

Amores, A., Melnichenko, O., & Maximenko, N. (2017). Coherent mesoscale eddies in the North Atlantic subtropical gyre: 3-D structure and transport with application to the salinity maximum. *Journal of Geophysical Research: Oceans*, *122*(1), 23–41. https://doi.org/10.1002/2016JC012256

Ardhuin, F., Gille, S. T., Menemenlis, D., Rocha, C. B., Rascle, N., Chapron, B., et al. (2017). Small-scale open ocean currents have large effects on wind wave heights. *Journal of Geophysical Research: Oceans*, *122*(6), 4500–4517. https://doi.org/10.1002/2016JC012413

AVISO. (2020). Gridded wind/wave products [Dataset]. *AVISO+*. Retrieved from https://www.aviso.altimetry.fr/en/data/products/wind/wave-products/mswh/mwind.html

AVISO. (2021). Jason-3 Geophysical Data Records (GDR), delayed-time [Dataset]. *AVISO+*. Retrieved from https://www.aviso.altimetry.fr/en/data/products/wind/wave-products/gdr-ogdr-osdr-ra2-wwv.html

AVISO. (2022). Mesoscale eddy trajectories atlas (META3.2 DT) [Dataset]. *Produced by SSALTO/DUACS and distributed by AVISO+ with support from CNES. Collaboration with IMEDEA*. https://doi.org/10.24400/527896/a01-2022.005.220209

Bignalet-Cazalet, F., Picot, N., Desai, S., Scharroo, R., & Egido, A. (2021). Jason-3 products handbook (Vol. *2*(1), pp. 1–73). SALP-MU-M-OP-16118-CN. https://www.aviso.altimetry.fr/en/data/products/wind/wave-products/gdr-ogdr-osdr-ra2-wwv.html

Booij, N., Holthuijsen, L. H., & Ris, R. C. (1996). The "SWAN" wave model for shallow water. *Coastal Engineering*, *1996*, 668–676. https://doi.org/10.1061/9780784402429.053

Casas-Prat, M., Hemer, M. A., Dodet, G., Morim, J., Wang, X. L., Mori, N., et al. (2024). Wind-wave climate changes and their impacts. *Nature Reviews Earth & Environment*, *5*(1), 23–42. https://doi.org/10.1038/s43017-023-00502-0

Chelton, D. B., Schlax, M. G., & Samelson, R. M. (2011). Global observations of nonlinear mesoscale eddies. *Progress in Oceanography*, *91*(2), 167–216. https://doi.org/10.1016/j.pocean.2011.01.002

Chen, G., Han, G., & Yang, X. (2019). On the intrinsic shape of oceanic eddies derived from satellite altimetry. *Remote Sensing of Environment*, *228*, 75–89. https://doi.org/10.1016/j.rse.2019.04.011

Cheng, T., Chen, Z., Li, J., & Babanin, A. V. (2025). Data and code for Mesoscale Eddy currents reshape the spatial distribution of wave height in the Southern Ocean [Dataset]. *figshare*. https://doi.org/10.6084/m9.figshare.30944852

Cheng, T., Chen, Z., Li, J., Xu, Q., & Yang, H. (2023). Characterizing the effect of ocean surface currents on Advanced Scatterometer (ASCAT) winds using open ocean moored buoy data. *Remote Sensing*, *15*(18), 4630. https://doi.org/10.3390/rs15184630

Copernicus Marine Service (CMEMS). (2025a). Global Ocean gridded L4 sea surface heights and derived variables reprocessed 1993 ongoing [Dataset]. *Copernicus Marine Data Store (MDS)*. https://doi.org/10.48670/moi-00148

Copernicus Marine Service (CMEMS). (2025b). Global Ocean waves reanalysis [Dataset]. *Copernicus Marine Data Store (MDS)*. https://doi.org/10.48670/moi-00022

Dickinson, S., Kelly, K. A., Caruso, M. J., & McPhaden, M. J. (2001). Comparisons between the TAO buoy and NASA scatterometer wind vectors. *Journal of Atmospheric and Oceanic Technology*, *18*(5), 799–806. https://doi.org/10.1175/1520-0426(2001)018<0799:cbttba>2.0.co;2

Echevarria, E. R., Hemer, M. A., & Holbrook, N. J. (2021). Global implications of surface current modulation of the wind-wave field. *Ocean Modelling*, *161*, 101792. https://doi.org/10.1016/j.ocemod.2021.101792

Fedor, L. S., & Brown, G. S. (1982). Waveheight and wind speed measurements from the SEASAT radar altimeter. *Journal of Geophysical Research*, *87*(C5), 3254–3260. https://doi.org/10.1029/JC087iC05p03254

Frenger, I., Gruber, N., Knutti, R., & Münnich, M. (2013). Imprint of Southern Ocean eddies on winds, clouds and rainfall. *Nature Geoscience*, *6*(8), 608–612. https://doi.org/10.1038/ngeo1863

Gourrion, J., Vandemark, D., Bailey, S., Chapron, B., Gommenginger, G. P., Challenor, P. G., & Srokosz, M. A. (2002). A two-parameter wind speed algorithm for Ku-band altimeters. *Journal of Atmospheric and Oceanic Technology*, *19*(12), 2030–2048. https://doi.org/10.1175/1520-0426(2002)019<2030:ATPWSA>2.0.CO;2

Hanley, K. E., Belcher, S. E., & Sullivan, P. P. (2010). A global climatology of wind–wave interaction. *Journal of Physical Oceanography*, *40*(6), 1263–1282. https://doi.org/10.1175/2010JPO4377.1

Hauser, D., Tison, C., Amiot, T., Delaye, L., Corcoral, N., & Castillan, P. (2017). SWIM: The first spaceborne wave scatterometer. *IEEE Transactions on Geoscience and Remote Sensing*, *55*(5), 3000–3014. https://doi.org/10.1109/TGRS.2017.2658672

He, Q., Zhan, H., Cai, S., & Zha, G. (2016). On the asymmetry of eddy-induced surface chlorophyll anomalies in the southeastern Pacific: The role of eddy-Ekman pumping. *Progress in Oceanography*, *141*, 202–211. https://doi.org/10.1016/j.pocean.2015.12.012

Hersbach, H., & Bidlot, J. R. (2008). The relevance of ocean surface current in the ECMWF analysis and forecast system. In *Proceedings from the ECMWF workshop on atmosphere-ocean interaction*. ECMWF.

Janssen, P. A. E. M. (1991). Quasi-linear theory of wind-wave generation applied to wave forecasting. *Journal of Physical Oceanography*, *21*(11), 1631–1642. https://doi.org/10.1175/1520-0485(1991)021<1631:qltoww>2.0.co;2

Kelly, K. A., Dickinson, S., McPhaden, M. J., & Johnson, G. C. (2001). Ocean currents evident in satellite wind data. *Geophysical Research Letters*, *28*(12), 2469–2472. https://doi.org/10.1029/2000GL012610

Komen, G. J., Cavaleri, L., Donelan, M., Hasselmann, K., Hasselmann, S., & Janssen, P. (1994). *Dynamics and modelling of ocean waves*. Cambridge University Press.

Law-Chune, S., Aouf, L., Dalphinet, A., Levier, B., Drillet, Y., & Drevillon, M. (2021). WAVERYS: A CMEMS global wave reanalysis during the altimetry period. *Ocean Dynamics*, *71*(3), 357–378. https://doi.org/10.1007/s10236-020-01433-w

Lin, X., Zhai, X., Wang, Z., & Munday, D. R. (2018). Mean, variability, and trend of Southern Ocean wind stress: Role of wind fluctuations. *Journal of Climate*, *31*(9), 3557–3573. https://doi.org/10.1175/JCLI-D-17-0481.1

Lindzen, R. S., & Nigam, S. (1987). On the role of sea surface temperature gradients in forcing low-level winds and convergence in the tropics. *Journal of the Atmospheric Sciences*, *44*(17), 2418–2436. https://doi.org/10.1175/1520-0469(1987)044<2418:otross>2.0.co;2

Ma, J., Xu, H., Dong, C., Lin, P., & Liu, Y. (2015). Atmospheric responses to oceanic eddies in the Kuroshio Extension region. *Journal of Geophysical Research: Atmospheres*, *120*(13), 6313–6330. https://doi.org/10.1002/2014JD022930

Marechal, G., & de Marez, C. (2022). Variability of surface gravity wave field over a realistic cyclonic eddy. *Ocean Science*, *18*(5), 1275–1292. https://doi.org/10.5194/os-18-1275-2022

Patara, L., Böning, C. W., & Biastoch, A. (2016). Variability and trends in Southern Ocean eddy activity in 1/12° ocean model simulations. *Geophysical Research Letters*, *43*(9), 4517–4523. https://doi.org/10.1002/2016GL069026

Pegliasco, C., Delepoulle, A., Mason, E., Morrow, R., Faugère, Y., & Dibarboure, G. (2022). META3.1exp: A new global mesoscale eddy trajectory atlas derived from altimetry. *Earth System Science Data*, *14*(3), 1087–1107. https://doi.org/10.5194/essd-14-1087-2022

Pérez-Santos, I., Seguel, R., Schneider, W., Linford, P., Donoso, D., Navarro, E., et al. (2019). Synoptic-scale variability of surface winds and ocean response to atmospheric forcing in the eastern austral Pacific Ocean. *Ocean Science*, *15*(5), 1247–1266. https://doi.org/10.5194/os-15-1247-2019

Pujol, M. I., Faugère, Y., Taburet, G., Dupuy, S., Pelloquin, C., Ablain, M., & Picot, N. (2016). DUACS DT2014: The new multi-mission altimeter data set reprocessed over 20 years. *Ocean Science*, *12*(5), 1067–1090. https://doi.org/10.5194/os-12-1067-2016

Quilfen, Y., & Chapron, B. (2019). Ocean surface wave-current signatures from satellite altimeter measurements. *Geophysical Research Letters*, *46*(1), 253–261. https://doi.org/10.1029/2018GL081029

Souza, J. M. A. C., Chapron, B., & Autret, E. (2014). The surface thermal signature and air–sea coupling over the Agulhas rings propagating in the South Atlantic Ocean interior. *Ocean Science*, *10*(4), 633–644. https://doi.org/10.5194/os-10-633-2014

Sun, W., Dong, C., Wang, R., Liu, Y., & Yu, K. (2017). Vertical structure anomalies of oceanic eddies in the Kuroshio Extension region. *Journal of Geophysical Research: Oceans*, *122*(2), 1476–1496. https://doi.org/10.1002/2016JC012226

Tan, K., Xie, L., Bai, P., Zheng, Q., Li, J., Xu, Y., & Li, M. (2023). Modulation effects of mesoscale eddies on sea surface wave fields in the South China Sea derived from a wave spectrometer onboard the China-France Ocean Satellite. *Journal of Geophysical Research: Oceans*, *128*(1), e2021JC018088. https://doi.org/10.1029/2021JC018088

Tolman, H. L. (1990). The influence of unsteady depths and currents of tides on wind-wave propagation in shelf seas. *Journal of Physical Oceanography*, *20*(8), 1166–1174. https://doi.org/10.1175/1520-0485(1990)020<1166:tiouda>2.0.co;2

19448007, 2026, 8, Downloaded from https://agupubs.onlinelibrary.wiley.com/doi/10.1029/2025GL119526 by Zhaohui Chen - Ocean University Of China , Wiley Online Library on [11/04/2026]. See the Terms and Conditions (https://onlinelibrary.wiley.com/terms-and-conditions) on Wiley Online Library for rules of use; OA articles are governed by the applicable Creative Commons License

Villas Bôas, A. B., Cornuelle, B. D., Mazloff, M. R., Gille, S. T., & Ardhuin, F. (2020). Wave–current interactions at meso- and submesoscales: Insights from idealized numerical simulations. *Journal of Physical Oceanography*, *50*(12), 3483–3500. https://doi.org/10.1175/JPO-D-20-0151.1

Wallace, J. M., Mitchell, T. P., & Deser, C. (1989). The influence of sea-surface temperature on surface wind in the eastern equatorial Pacific: Seasonal and interannual variability. *Journal of Climate*, *2*(12), 1492–1499. https://doi.org/10.1175/1520-0442(1989)002<1492:tiosst>2.0.co;2

Wang, H., Qiu, B., Liu, H., & Zhang, Z. (2023). Doubling of surface oceanic meridional heat transport by non-symmetry of mesoscale eddies. *Nature Communications*, *14*(1), 5460. https://doi.org/10.1038/s41467-023-41294-7

Young, I. R., Fontaine, E., Liu, Q., & Babanin, A. V. (2020). The wave climate of the Southern Ocean. *Journal of Physical Oceanography*, *50*(5), 1417–1433. https://doi.org/10.1175/JPO-D-20-0031.1

Zieger, S., Vinoth, J., & Young, I. R. (2009). Joint calibration of multiplatform altimeter measurements of wind speed and wave height over the past 20 years. *Journal of Atmospheric and Oceanic Technology*, *26*(12), 2549–2564. https://doi.org/10.1175/2009JTECHA1303.1

19448007, 2026, 8, Downloaded from https://agupubs.onlinelibrary.wiley.com/doi/10.1029/2025GL119526 by Zhaohui Chen - Ocean University Of China , Wiley Online Library on [11/04/2026]. See the Terms and Conditions (https://onlinelibrary.wiley.com/terms-and-conditions) on Wiley Online Library for rules of use; OA articles are governed by the applicable Creative Commons License